Component assembly with shape memory polymer fastener for microrobots

2014 Smart Mater. Struct. 23 015011

(http://iopscience.iop.org/0964-1726/23/1/015011)

IOP Publishing Smart Materials and Structures
Smart Mater. Struct. **23** (2014) 015011 (12pp) doi:10.1088/0964-1726/23/1/015011

Component assembly with shape memory polymer fastener for microrobots

Ji-Suk Kim, Dae-Young Lee, Je-Sung Koh, Gwang-Pil Jung and Kyu-Jin Cho

Department of Mechanical and Aerospace Engineering, Seoul National University, Seoul 151-742, Korea

E-mail: kjcho@snu.ac.kr

Received 27 August 2013, in final form 23 October 2013
Published 10 December 2013

Abstract

Adhesives are generally used for the assembly of microrobots, whereas bolts, screws, or rivets are used for larger robots. Although adhesives are easy to apply, lightweight, and small, they cannot be used for repeated assembly and disassembly of parts. In this paper, we present a novel microfastener composed of a polyurethane-based shape memory polymer (SMP) that is lightweight and small but that is easily detached for disassembly. This was achieved by using the shape recovery and modulus change of the SMP. A sheet of macromolded SMP was laser machined into an I-beam-shaped rivet, and notches were added to the structure to prevent stress concentration. Pull-off tests showed that, as the notch radius increased, the disengagement strength of the rivet fastener decreased and the reusability increased. Through the elastoplastic model, a single SMP rivet was calculated to have maximum disengagement strength of 150 N cm^{-2} in the elastic range, depending on the notch radius. The fasteners were applied to a jumping microrobot. The legs and body were assembled with ten fasteners, which showed no permanent deformation after impact during jumping movements. The legs were easily replaced with ones of different stiffness by heating the engaged sites to make the fasteners compliant and detachable. The proposed detachable SMP microfasteners are particularly useful for testing the isolated performance of microrobot components to determine the optimal designs for these components.

Keywords: shape memory polymer fastener, microrobot, releasable assembly, blind rivet, microfastener

(Some figures may appear in colour only in the online journal)

1. Introduction

Shape memory polymers (SMPs) are polymeric smart materials that have the ability to return from a deformed state to their original shape when induced by an external stimulus such as temperature change [1]. SMPs have two distinctive properties. First, they are temporarily deformed above the glass transition temperature (T_g), and then subsequently cooled, while maintaining the deformation to below T_g. They recover their original shape when reheated above T_g. Second, the elastic moduli of SMPs decrease by three orders of magnitude when they change from the glassy to the rubbery state.

If the above-mentioned two properties of SMPs could be exploited, they would offer users considerable advantages over other polymers for fasteners. For example, the shape recovery of SMPs could be used to produce blind rivet fasteners that would be remotely activated by external stimulus without the need to apply any mechanical force. In addition, a drastic modulus change of SMPs during transition would enable the manufacture of fasteners requiring low engagement and disengagement forces. Only a few studies, however, have attempted to use SMPs to manufacture releasable fasteners. Cornerstone Research Group Inc. developed shape memory 'smart' fasteners [2]. When two sides of the group's mushroom-shaped SMP fasteners were heated, they became flexible, thus enabling snap-on attachment. Once fastened, they returned to a rigid state, locking the fasteners in place. In another study, it was proposed that SMPs could have a memorized 'hook' shape

and be used as a hook-and-loop fastener to reduce the pull-off force by heating them above T_g [3]. Flanigan *et al* proposed a wide range of conceptual applications of SMPs as releasable fasteners that change the geometry of the shaft between the release geometry and the attachment geometry without applying a mechanical force [4].

Studies on SMP-based fasteners indicate that these fasteners perform better on a small scale because SMPs generally have low thermal conductivity. Given the same amount of energy, the smaller the SMP-based fastener, the shorter is the required activation time. Therefore, although it can be manufactured to a variety of sizes, an SMP-based fastener may also be used as an assembly component to engage various small parts.

SMP fasteners could be used in the releasable assembly of parts of a microrobot. Microrobots are usually made with dimensions of the order of 1 cm, and their parts are often made of thin, strong, and lightweight materials such as carbon-fiber-reinforced polymer (CFRP) or glass-fiber-reinforced polymer (GFRP) [5]. They are normally assembled using adhesives, and for simplicity, current manufacturing processes of fiber-reinforced polymer microrobots do not include a releasable assembly process. However, as fabrication technologies are developed further and the mechanisms of microrobots become more complicated, demand will increase for a replacement for cyanoacrylates, magnets, or Scotch tape, which are either nonrepeatable, heavy, or weak. For these reasons, many researchers have attempted to adopt alternative connecting methods in various robots. A releasable drive shaft developed by Wood *et al* was a key component of a micro air vehicle to facilitate the interchange of parts and to study isolated performance [6]. Kovač *et al* also used brass axes to join the aluminum legs of a 7 g jumping robot [7]. Magnets are favored in particular for reconfigurable modular or origami robots [8, 9]. Fearing *et al* constructed a polyethylene-based reusable microconnector to ensure reusability, a low-engaged profile, and rapid assembly [10]. The aim of this microconnector is to assemble the components of a microrobot repeatedly, and the connectors are fabricated on the two surfaces to be engaged. The main distinction is that the microconnectors are engaged by interdigitating the ridges on the two surfaces, whereas the SMP rivet fasteners engage two parts by inserting the rivet through a small hole and expanding their arms to hold the parts in place.

In this paper, we propose a novel SMP-based fastener for microrobots. Among many classical methods of mechanically joining two parts together, a rivet design was chosen for the SMP-based fastener because it can produce semipermanent joints between dissimilar materials of a wide variety of shapes and sizes [11]. Moreover, a rivet design does not require any type of adhesive backing that is found in a hook-and-loop design, e.g., Velcro, but requires only small premade holes in the parts. The SMP rivet fastener has three distinctive properties. First, it enables blind riveting because of its material property. Second, it requires no mechanical force or extra tools for the blind riveting. Third, it is easily detachable because it becomes compliant when heated. Unlike conventional blind rivets, the SMP blind rivet can be remotely triggered by heat without applying any mechanical force. This is particularly favorable when users need to assemble several parts simultaneously, namely, self-assembly of modular robots. Finally, the fact that the SMP rivet fastener is detachable in the rubbery state and reusable differentiates it from conventional rivet fasteners because conventional rivets provide users with only irreversible engagement.

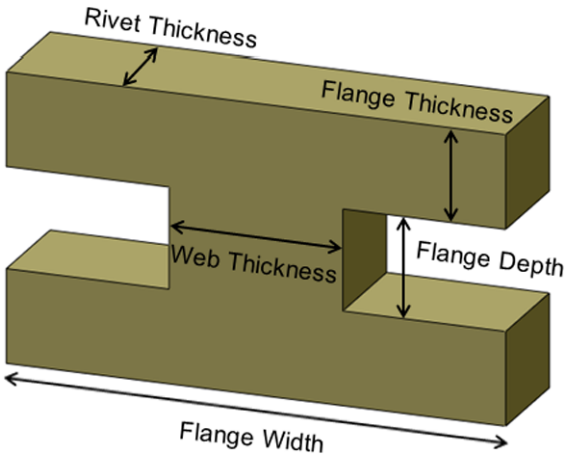

Figure 1. Elements of the basic rivet.

This paper investigates the design and modeling of the SMP rivet fastener and studies the relationships between disengagement strength and reusability in various designs. In its fabrication, laser processing enables the manufacture of SMP rivets with dimensions of the order of 1 mm and the adjustment of shapes and dimensions when necessary. SMP rivets specifically designed and fabricated in this manner were applied to the mesoscale flea-inspired robot developed by Cho *et al* [12]. The flea robot is composed of a single body part and two leg parts, and the stiffness of the robot legs may affect the robot's jumping capability. Because the leg parts are assembled using SMP rivet fasteners, they can be easily detached and replaced, preventing deterioration in experimental accuracy due to old leg parts and improving the efficient use of research time and materials. Therefore, the SMP rivet fastener is an attractive assembly component for researchers looking for an optimal robot design or for those dealing with fragile mechanical parts.

2. Design

2.1. Basic design and assembly process

Among the many rivet designs that could be made using 2D fabrication, the I-beam-shaped fastener is one of the most basic. The terminology of a general I-beam is used to describe the I-beam-shaped fastener in figure 1. The flange of the I-beam in figure 1 could work as a foot of a rivet, and the web of the I-beam parallels a shank of a rivet. Figure 2 shows how the engagement process works with this basic I-beam-shaped fastener. This fastener works as a low-profile adhesive; it should also be reusable because it becomes highly compliant and detachable when heated. It can be used to join parts

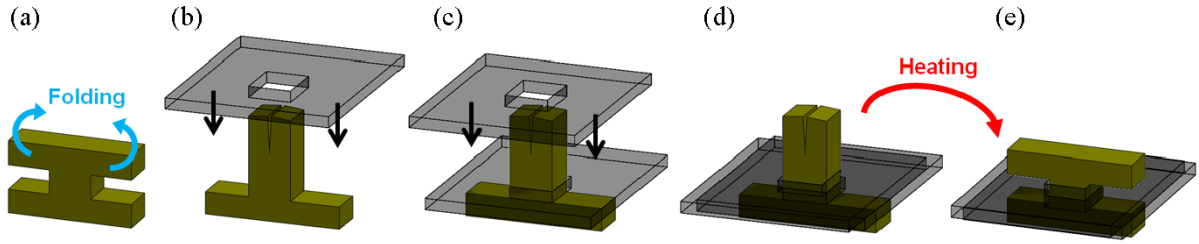

Figure 2. Schematic process flow for the component assembly using the SMP I-beam rivet: (a) the rivet flanges are folded at room temperature, (b) the lower part with a premade hole is inserted, (c) the upper part with the hole is inserted, (d) the rivet is activated by an external heat source, and (e) the rivet recovers its original shape to mechanically join two parts.

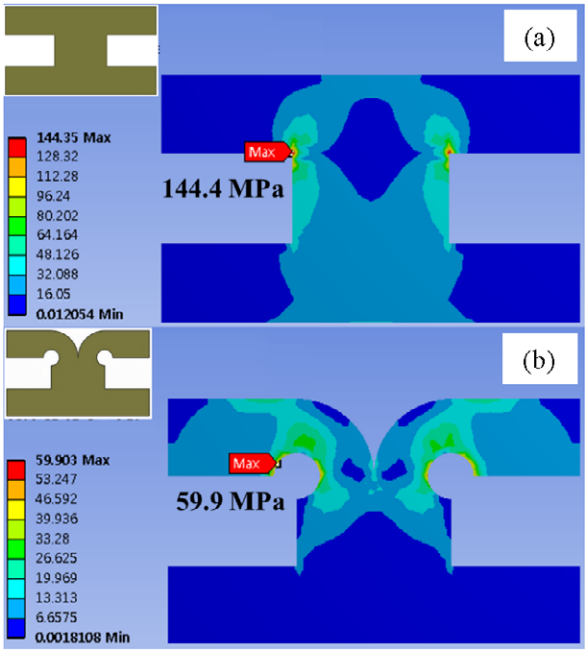

Figure 3. Stress distribution predicted by the finite element simulation of (a) the basic rivet design and (b) the modified design, when the same amount of vertical displacement was applied to both flanges of the two rivets.

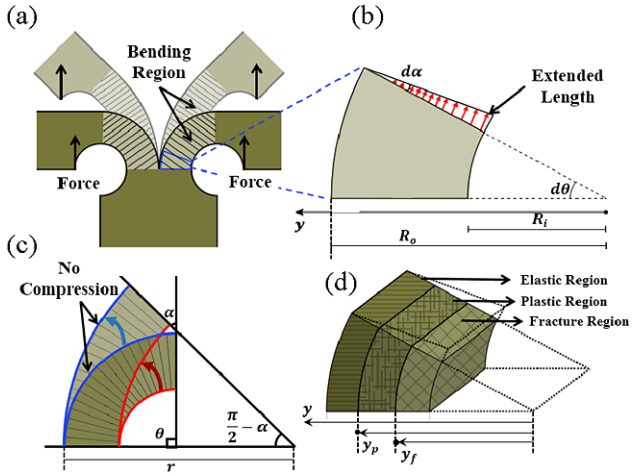

Figure 4. Analysis of the rivet structure for modeling. (a) Deformation of the whole rivet under an external force and the assumed bending region. (b) Infinitesimal element of the rivet. (c) Changes of lengths in the bending region. (d) Cross-sectional analysis of the stress distribution.

through the blind-riveting method, by making use of the shape memory effect when these parts are highly inaccessible and difficult to assemble with conventional assembly components such as bolts and nuts.

However, as shown in figure 3(a), on the basis of commercially available simulation software (ANSYS), I-beam-shaped fasteners with straight flanges are expected to have limitations because stress concentration occurs at the middle of the flange and at points where the flange and the web meet during folding. These stress concentration points could cause cracks or hinder the rivet insertion process. To avoid the occurrence of these phenomena, the design of the basic rivet shape must be changed. The modified basic rivet design in figure 3(b) has two notches at two points where the flanges and the web meet and a large notch at the top of the web. The stress is properly distributed around the notches, and the insertion process becomes easier at the expense of a certain amount of reduction in disengagement strength. However, the amount of reduction of stress in the design modification is unpredictable unless there is a model that shows behavior similar to that of the actual SMP rivet and explains the changes in disengagement strength and reusability as the size of the notches changes.

2.2. Model of the disengagement strength

The disengagement strength of the modified SMP rivet fastener was analyzed using conventional elastoplastic beam theory [13]. The structural analysis and modeling of the SMP rivet can be used to guide the design of SMP rivets.

In the analysis, the following assumptions are made: (1) bending occurs only in the shaded region in figure 4(a); (2) the shaded region can only be extended and cannot be compressed, as shown in figure 4(c); (3) there are at most three regions during disengagement—the elastic, plastic, and fracture regions.

The first assumption concerns the bending region. Although other areas of the flange also undergo deformation, the amount of deformation is negligible. The second assumption concerns compression. This assumption arises because the consistent upward force would induce tension in the curved area more dominantly than compression would. The third assumption concerns the stress profile. In the elastic

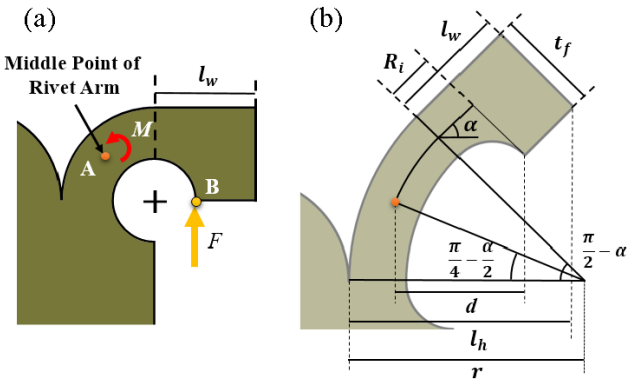

Figure 5. Geometrical analysis of the deformation of the rivet. (a) Schematic drawing of the applied force and moment. (b) Structure of a flange in a deformed state.

Table 1. Nomenclature.

Symbol	Definition
ε	Total elongation strain
ε_p	Strain when plastic deformation starts
ε_f	Strain when fracture starts
y	Variable on radial axis
y_p	Starting point of plastic region
y_f	Starting point of failure region
R_i	Inner radius of the notch
R_o	Outer radius of the notch
r	Outer radius of the deformed notch
t_r	Thickness of the rivet
t_f	Height of the flange
l_w	Total length of the flange
l_h	Projection length of the deformed flange
α	Angular deformation
θ	Initial angle of the bending region
σ_{max}	Maximum stress on the cross section
d	Length of the moment arm

region, the stress has a linear relation with strain, whereas the stress in the plastic region is assumed to be constant [14]. In the fracture region, the stress reaches zero as the strain exceeds a certain limit and the structure is broken. With these assumptions, the SMP rivet model was derived to estimate the disengagement strength of real SMP rivets.

The definitions of symbols used in equations can be found in table 1, and the geometrical definitions are shown in figures 4 and 5.

The strain of the rivet as a function of y can be obtained from geometrical analysis, as shown in figure 4(b), and the following equation.

$$\varepsilon = \frac{\text{Extended length}}{\text{Original length}} = \frac{R_o - y}{y} \cdot \frac{d\alpha}{d\theta} \approx \frac{R_o - y}{y} \cdot \frac{\alpha}{\theta} \qquad \left(\theta = \frac{\pi}{2}\right). \tag{1}$$

On the basis of the assumptions mentioned earlier, the stress in the cross section can be classified into three regions depending on the strain. The strain when plastic deformation starts, $\varepsilon_{plastic}$, and the strain when fracture starts, $\varepsilon_{fracture}$, can be obtained through a tensile test on the SMP specimen.

$$\sigma = \begin{cases} E\varepsilon & (\varepsilon < \varepsilon_{plastic}) \\ \sigma_{max} & (\varepsilon_{plastic} < \varepsilon < \varepsilon_{fracture}) \\ 0 & (\varepsilon_{fracture} < \varepsilon). \end{cases} \tag{2}$$

From the above stress profile, the rivets are expected to remain in the elastic region before $\varepsilon_{plastic}$, and they must stay in this region when actually applied to a microrobot. After they pass the elastic region, they pass through the plastic region, where their flanges have permanent deformation but the engaged parts remain held together. After this process, some of the rivets will be in the fracture region, and the others will remain in the plastic region until disengagement, depending on the notch radius. Because the notch radius determines the final strain of the rivet at disengagement, there must be a 'critical notch radius' that determines whether the rivets will have a fracture region.

The starting points of each region, y_p and y_f, can also be calculated from equation (1) as follows:

$$y_p = \frac{R_o}{1 + \varepsilon_p \frac{\pi}{2\alpha}} \qquad (\text{when } y_p \geq R_i) \tag{3}$$

$$y_f = \frac{R_o}{1 + \varepsilon_f \frac{\pi}{2\alpha}} \qquad (\text{when } y_f \geq R_i). \tag{4}$$

The moment M caused by the internal stress at the cross section is calculated by integrating the stress in each region in equation (2) as follows:

$$\begin{aligned} M &= \int_{R_i}^{R_o} \sigma (R_o - y) t \, dy = \int_{y_p}^{R_o} E\varepsilon (R_o - y) t \, dy \\ &\quad + \int_{y_f}^{y_p} \sigma_{max} (R_o - y) t \, dy + \int_{R_i}^{y_f} 0 \cdot (R_o - y) t \, dy \\ &= \frac{2\alpha E t}{\pi} \left\{ R_o^2 \ln \frac{R_o}{y_p} - 2R_o (R_o - y_p) + \frac{1}{2}(R_o^2 - y_p^2) \right\} \\ &\quad + \sigma_{max} t \left\{ R_o (y_p - y_f) - \frac{1}{2}(y_p^2 - y_f^2) \right\}. \end{aligned} \tag{5}$$

The moment caused by the applied force is calculated through geometrical analysis of the rivet, as shown in figure 5. In this analysis, it is assumed that the force is always applied at the lowest point of the flanges, point B in figure 5(a), and the average deformation is assumed to be the same as that of the midline of the flange, on which point A lies, as shown in figure 5(a). The outer radius of the deformed notch, r, can be obtained from equation (6), which is derived from figure 5(b). The moment arm from the middle point of the flange to the force-applied point B is calculated using equation (7), and the applied moment is calculated using equation (8).

$$r = \frac{\frac{\pi}{2} R_o}{\frac{\pi}{2} - \alpha} \tag{6}$$

$$d = \left(r - \frac{R_o - R_i}{2} \right) \left\{ \cos\left(\frac{\pi}{4} - \frac{\alpha}{2} \right) - \cos\left(\frac{\pi}{2} - \alpha \right) \right\}$$

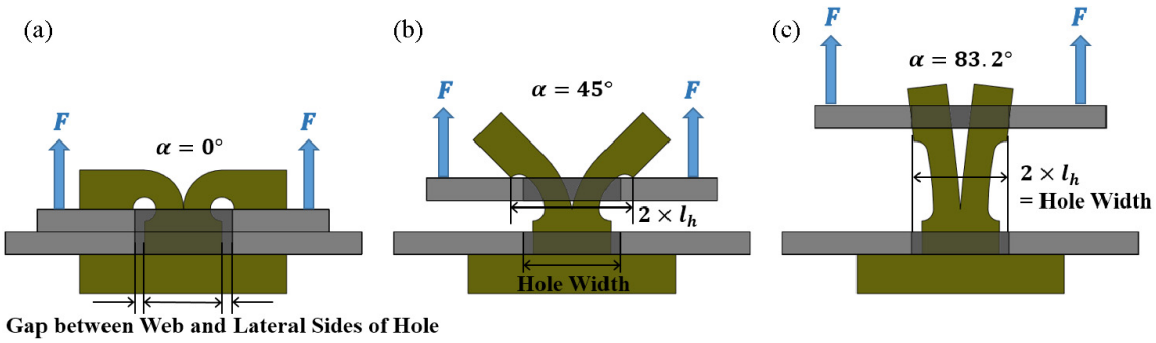

Figure 6. Schematic process flow for disengagement of two parts. (a) Two parts are engaged by the modified SMP rivet fastener, and a gap exists between the web and the lateral sides of the hole. (b) Angular deformation reaches 45° due to external force. (c) When the angular deformation reaches 83.2°, the rivet flanges can no longer withstand external forces and let the upper part fall out.

$$+ R_i \cos\alpha + \left(\frac{R_i + R_o}{2}\right)\sin\alpha \tag{7}$$

$$M_{applied} = F \cdot d = F \cdot \left[\left(r - \frac{R_o - R_i}{2}\right) \times \left\{\cos\left(\frac{\pi}{4} - \frac{\alpha}{2}\right) - \cos\left(\frac{\pi}{2} - \alpha\right)\right\} + R_i \cos\alpha + \left(\frac{R_i + R_o}{2}\right)\sin\alpha\right]. \tag{8}$$

Because the moment caused by the internal stress is equal to the moment caused by the applied force, the disengagement force can be calculated as follows:

$$F = \left(\frac{2\alpha E t}{\pi}\left\{R_o^2 \ln\frac{R_o}{y_p} - 2R_o(R_o - y_p) + \frac{1}{2}(R_o^2 - y_p^2)\right\} + \sigma_{max} t\{R_o(y_p - y_f) - \tfrac{1}{2}(y_p^2 - y_f^2)\}\right) \times \left(\left(r - \frac{R_o - R_i}{2}\right)\left\{\cos\left(\frac{\pi}{4} - \frac{\alpha}{2}\right) - \cos\left(\frac{\pi}{2} - \alpha\right)\right\} + R_i \cos\alpha + \left(\frac{R_i + R_o}{2}\right)\sin\alpha\right)^{-1}. \tag{9}$$

From equation (9), it can be seen that the external force is a function of R_o, R_i, t, y_p, y_f, and α, and only the elastic modulus E is predetermined by the material properties. However, once the rivet design is settled, it is easy to obtain a direct relationship between the applied force F and the angular deformation α by substituting equations (3) and (4) into equation (9). According to the rivet design, the fracture region may or may not appear at the cross section of the flange during disengagement. The notch radius R_i is closely related to whether or not fracture occurs, and it also affects the disengagement force; hence, it is reasonable to set R_i as a dominant design parameter.

When the notch is smaller than the 'critical radius' explained above, fracture occurs during disengagement, and the maximum disengagement force is the external force that is applied to the rivet immediately before fracture. This happens even before the flanges are fully folded.

However, when the notch is larger than the critical size, failure does not occur even when the rivet is fully folded. In this case, the rivet withstands the maximum disengagement force when the angular deformation of flanges is sufficiently large to let the upper part fall out of the rivet. One noticeable fact is that the deformation angle is less than 90° because there should be a gap between the rivet web and the lateral sides of the hole in connected parts. This gap allows us to examine the individual performance of the rivet itself and avoid overestimation due to the friction between the rivet web and the lateral sides of the hole.

The final deformation angle can be geometrically analyzed from figure 6. It reveals that the connected part is detached when twice the projection length of the deformed flange, $2 \times l_h$, is equal to the width of the hole of the connected part, and the final angular deformation is calculated to be 83.2°. The projection length of the deformed flange, l_h, is obtained from the following equation, which is derived from figures 5(b) and 6.

$$l_h = r\left\{1 - \cos\left(\frac{\pi}{2} - \alpha\right)\right\} + l_w \cos\alpha + t_f \sin\alpha. \tag{10}$$

3. Fabrication

3.1. Raw materials

The materials used in this study included pellet type MM-5520 SMP from SMP Technologies Inc. (glass transition temperature 55 °C, as provided by the manufacturer). Although the provided instructions recommend injection molding to produce a sample [15], another fabrication method was chosen in this study because of the difficulties in demolding small products. As indicated in figure 7, macromolding and subsequent laser machining were considered to be superior to microinjection molding because, when using micromolding, microstructures can be seriously damaged during demolding, and the mold design must be modified every time the design requires modification [16]. For these reasons, macromolding and laser machining were used instead of injection molding for making microscale SMP rivets.

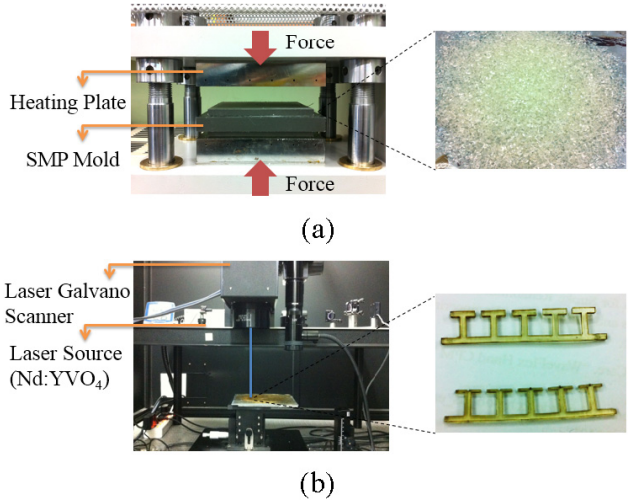

Figure 7. Manufacturing process for SMP rivet. (a) Macromolding the SMP plate with a heat press machine. (b) Cutting the SMP plate into a rivet shape with a laser machine.

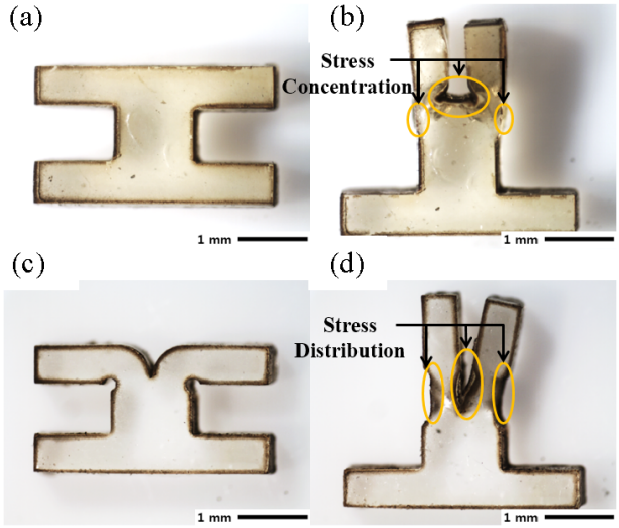

Figure 8. (a) Laser-machined I-beam. (b) I-beam rivet is folded. (c) Modified I-beam design. (d) Modified I-beam design is folded.

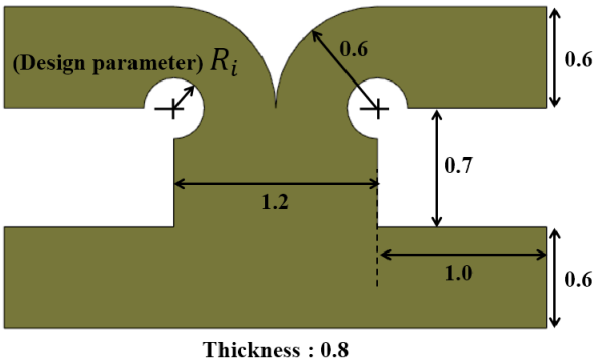

Figure 9. Detailed dimensions of the modified I-beam type and the design parameter (size in millimeters).

3.2. Macromolding process

To create an SMP plate that can be easily laser machined, a heat press machine and a rectangular mold were used. First, 30 g of pellets was poured into a steel mold with inner dimensions of 150 mm × 150 mm × 1 mm. A prelaid release film (WL5200B-P3-001-60″, provided by JetKorea Co., Ltd) must be present on the bottom of the mold to eliminate sticking problems during demolding. Because there are a large number of air bubbles inside the raw pellets, direct molding at the recommended temperature (at 205 °C) [17] would produce serious defects. Therefore, the pellets were heated in a mold inside the heat press machine as a preliminary process at a temperature above its melting point (at 250 °C) for approximately 10 min. When the pellets had become completely molten, another sheet of release film was laid upon the pellets. Finally, the mold lid was located, and then the recommended temperature (205 °C) and pressure (20 MPa) were applied with the heat press machine. In the macromolding process, an SMP plate of 800 μm thickness was fabricated.

3.3. Laser machining process

A Nd:YVO_4 laser system (Aptowave, USA; wavelength 355 nm, pulse duration 30 ns, repetition rate 100 kHz) was used to perform a cutting process on the 800 μm-thick SMP plate. Laser machining with 2.6 W of power, a scanner speed of 120 mm s^{-1}, and 180 repetitions enabled the generation of a fine cutting surface without damaging the polymer. If the plate is laser-processed 180 times without interruption, the affected area will become molten, and it will be difficult to obtain an intact desired shape [18, 19]. To allow each laser-processed shape sufficient time to cool, 50 identical shapes were marked successively, and each shape was processed only twice at any one time. This cycle was performed 90 times. The time required for one cycle was 14.5 s, and the estimated overall time was 21 min 45 s. Therefore, the required time for one rivet was approximately 26.1 s.

Figure 8(a) shows the laser-machined I-beam rivet. It can be seen that stress concentration actually occurred at three points when folded. Figure 8(c) shows the modified I-beam rivet. It can be seen that the stresses were successfully distributed by adding three notches at target points. To compare the results of the SMP beam-bending model with the behavior of the SMP rivet, detailed dimensions were designed, as shown in figure 9, and nine types of samples with differing design parameters were fabricated, as shown in figure 10.

4. Experiment

A uniaxial tensile test was carried out with a universal test machine (Instron 5940) on a laser-cut dog-bone specimen to determine the mechanical properties of the SMP rivet fastener. With the assumption that the working temperature of the rivets is room temperature (25 °C), the uniaxial tensile tests and pull-off tests were performed at this temperature. The thermomechanical properties of a thin film of polyurethane

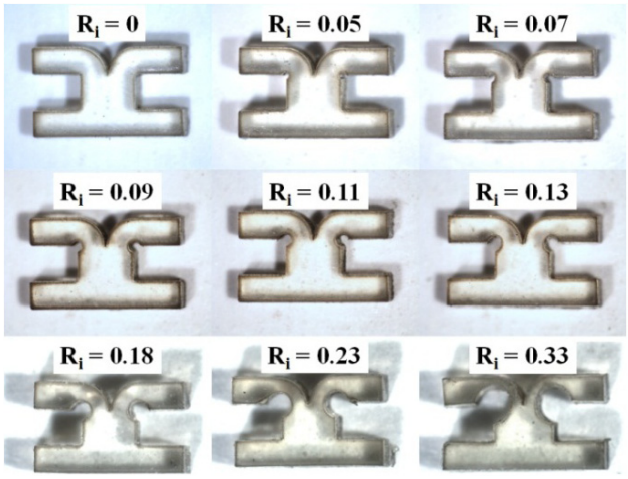

Figure 10. Nine laser-machined samples with differing notch radii. All other dimensions of these samples are the same as those in figure 9.

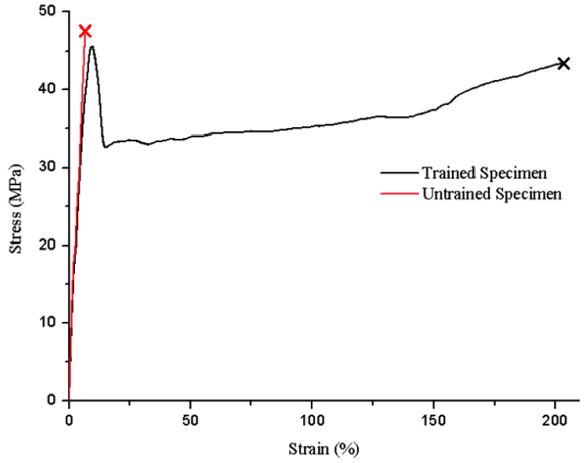

Figure 11. Stress–strain curve of the untrained and trained SMP specimen at room temperature.

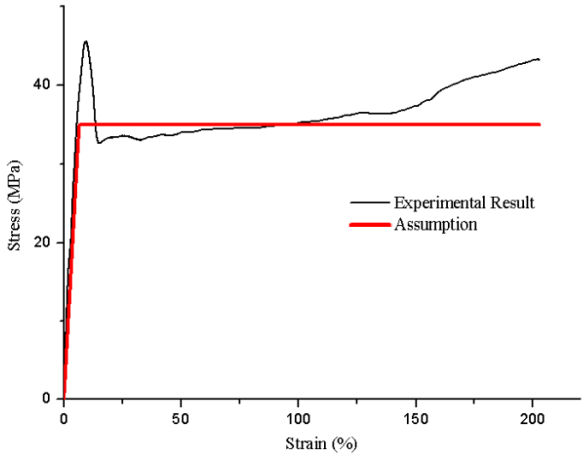

Figure 12. Stress–strain curve of the sample at room temperature and assumed stress–strain curve for modeling.

SMPs have been examined by earlier studies [20, 21]. Therefore, the change in mechanical properties of SMP rivets could be estimated by using the experimental results in these studies. In section 4.1, only the uniaxial tensile tests on dog-bone-shaped SMP specimens were conducted under the apprehension that the properties might be different from those provided by manufacturers due to the new fabrication method. The elastic modulus and tensile yield strength obtained in this experiment were used for ANSYS simulation and for the beam-bending model described in section 2. After the mechanical properties of SMP were identified, the disengagement strength of the laser-machined SMP rivet fasteners was tested using the same machine.

4.1. Basic material property measurement test

Dog-bone-shaped test samples were fabricated through the same process as for the SMP rivet fasteners—macromolding and laser machining—to ensure a consistent material property. As indicated by the red line in figure 11, the specimens without any treatment after laser machining—the untrained specimens—were brittle and subject to precracking at room temperature, which may occur in rivet structures too. This phenomenon may have resulted from residual stress in the SMP plate during macromolding, as specified in earlier studies [22]. To remove the internal stress, the specimens were immersed in hot water (70 °C) for a few seconds and dried. Because the immersion time was only a few seconds, the effect of moisture on the thermomechanical properties was negligible [23]. After training, the specimens showed relatively consistent and repeatable results at room temperature. The measured elastic modulus and tensile yield strength were 0.56 GPa and 46 MPa, respectively. As shown in figure 12, to simplify the modeling, the original elastic modulus of 0.56 GPa was used until 6.5% strain, and it was assumed that the stress remained 35 MPa until failure (200% strain) at 25 °C.

4.2. Disengagement strength measurement test

Figure 13 shows the experimental setup used to measure the disengagement strength of the SMP rivet fastener. Two CFRP sheets of thickness 350 μm were fabricated for engagement by SMP rivet fasteners. Two small holes were made at both ends of the upper CFRP part, through which two nylon-coated stainless-steel wires (0.012″) were inserted and gripped by upper pneumatic grips. On the lower CFRP part were two large holes for the bolts to fix the lower CFRP part on the bottom polycarbonate support, which was gripped by lower pneumatic grips.

The modified I-beam type was tested for disengagement strength and reusability at room temperature. Three copies of each of the nine samples were tested four times. The flanges of the SMP rivet fasteners were folded with tweezers at room temperature and were activated with hot water (80 °C) after insertion. The results shown in figure 14 indicate how the disengagement strength changed as the size of the notch and the trial number increased. The disengagement strength

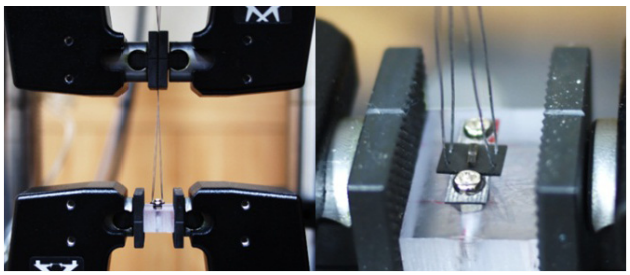

Figure 13. Pull-off test setup to measure the disengagement strength of the SMP rivet fastener.

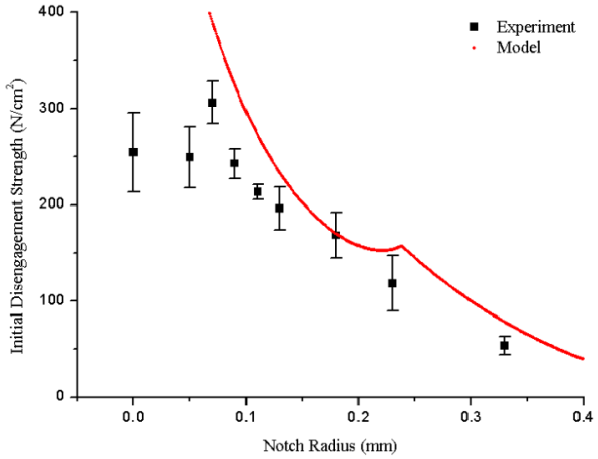

Figure 14. Measurement results of the initial disengagement strength of nine samples, and the maximum disengagement strength predicted by the model.

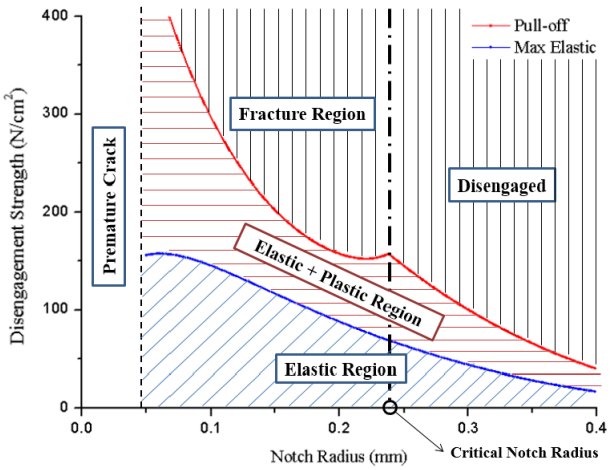

Figure 15. Distinct elastic, elastic and plastic, and fracture regions estimated by the model. The SMP rivet functions as a normal assembly component within the elastic region.

was obtained by dividing the detachment force by the area covered by the SMP rivet fastener (0.0256 cm^2). As expected, a direct correlation was found between notch radius and disengagement strength. In the first two samples, either there were no notches or the notches were so small that cracks were caused by stress concentration during the folding process, and thus the values of these two samples could be neglected. Except for these two samples, the disengagement strength was inversely proportional to the size of the notch.

For easy comparison of the actual values and those predicted by the beam-bending model, the initial disengagement strengths were plotted along with the values predicted by the model, as shown in figure 14. The first two points from experiments show great differences from the beam-bending model, since the disengagement strengths estimated by the model diverge when the notch size becomes smaller than 0.05 mm. The divergence is derived from the fact that the denominator, the moment arm from the middle point of the flange to the force-applied point, in equation (9) goes to zero as the notch size becomes smaller. In reality, there were premature cracking and unexpected deformations in structure. Therefore, the beam-bending model used in this study has limits—the minimum notch size of 0.05 mm. The maximum force is calculated, as stated in section 2, either when the flanges undergo failure or when their angular deformation reaches 83.23°, which is calculated with equation (10). As shown in figure 14, the disengagement strengths obtained from the experiment and those from the model were of the same order of magnitude, and the decreasing trend of disengagement strength with increasing notch radius was predicted well by the model.

Although the performance of each rivet design was estimated on the basis of the pull-off tests, the rivets must remain in the elastic region when they are actually applied to a microrobot. It is difficult to measure the final point of an elastic region through a tensile test because the boundaries of each region can be ambiguous during disengagement. However, the feasibility of the elastoplastic model has been confirmed above, thus enabling designers to use the model to estimate how much external force each rivet design can endure without permanent deformation in its structure. These values are plotted against the notch radius in figure 15. The blue-shaded region of the figure denotes the elastic region, which indicates the range of endurable external force according to notch radius. It is noticeable that rivets with small notches do not always offer the widest elastic region, because of premature cracking from stress concentration. As explained in section 2, a fracture region occurs when the notch radius is smaller than the critical value, whereas the other rivets are disengaged prior to fracture occurrence.

The reusability of rivets can be estimated from the trend line of each graph in figure 16(a). The trend lines were obtained using a least-squares approximation that minimizes the error between the four points and the least-squares line. The absolute values of the slopes of these trend lines are plotted against the notch radius in figure 16(b). The reusability of a rivet can be easily estimated from these values in the graphs. For example, if one rivet is tested that has a slope value of 0.2, we know that this rivet will lose its disengagement strength by approximately 20% in the next trial. Therefore, from the graph shown in figure 16(b), it is clear that the last four samples are highly repeatable because the slope of each graph decreases and reaches almost zero as the notch radius

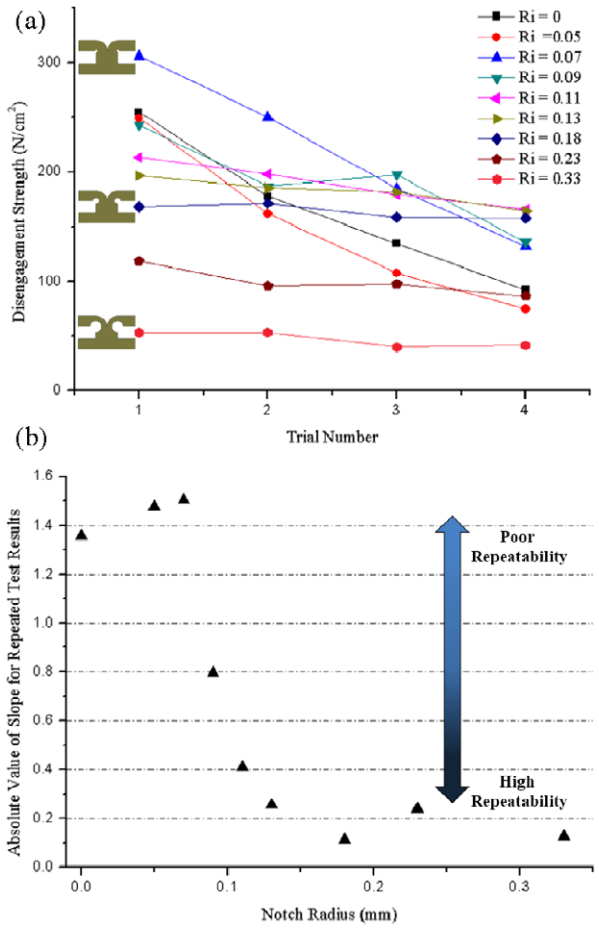

Figure 16. (a) Measurement results of disengagement strength and reusability for nine samples of the modified I-beam-type rivet. (b) Absolute value of slopes of samples in the graph versus notch radius. Reusability can be estimated from this graph. The smaller the value of the slope, the better is the reusability.

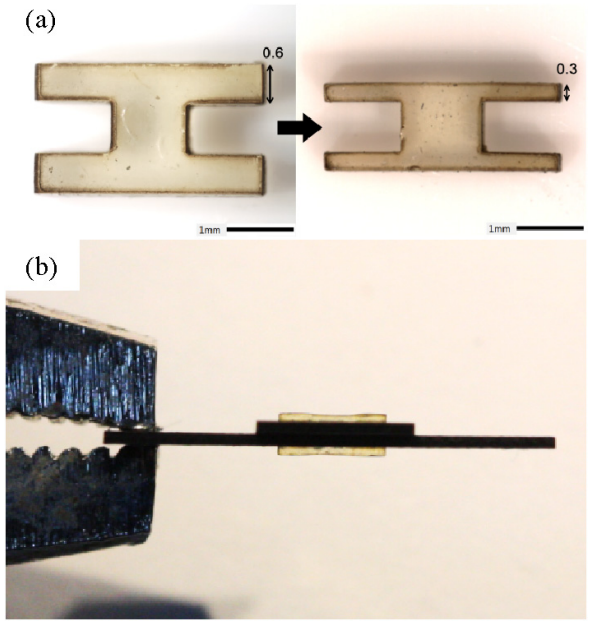

Figure 17. (a) Modification of an I-beam-shaped design to produce a low-profile connector. (b) Two CFRP parts are assembled via the low-profile I-beam-shaped SMP rivet fastener.

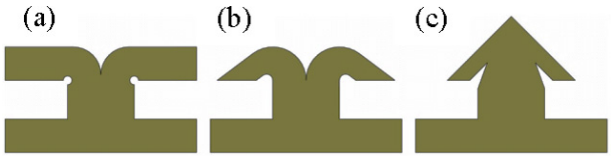

Figure 18. (a) I-beam-shaped rivet fastener. (b) Anchor-shaped rivet fastener. (c) Arrow-shaped rivet fastener.

increases. Despite the high reusability of the SMP rivet with large notches, its low maximum disengagement strength may limit actual application to a microrobot.

5. Variations of the rivet shape

The modified I-beam type is easy to model and offers low-profile engagement, as shown in figure 17; however, it is neither the most efficient shape nor the easiest form to handle. In more practical terms, the disengagement strength could be enhanced by modifying the web thickness or the flange angle of the rivets. The web thickness can be increased beyond the hole thickness so that the web can be deformed to be thinner than the hole before insertion and snugly fit into the hole after heating. The flanges can be angled downward so that the flanges can apply more pressure on the part. Besides, because the properties of an SMP rivet may vary depending on its specific design, it is worth attempting rivet shapes that are completely different from the basic I-beam type. On the basis of the results of many trials, we propose two more types—anchor type and arrow type—as shown in figures 18(b) and (c). Two variations of design were devised by considering variations of disengagement force, reusability, and ease of insertion. The second anchor-shaped fastener maximizes the effect of stress distribution and reusability by changing the flat flanges to curved ones, which facilitate easy insertion by giving it the appearance of a spearhead when fully folded. The other type was inspired by conventional plastic rivet, or 'snap-fit', fasteners. It uses a hook- or catch-like geometry that deflects when beginning to be inserted into a hole and recovers its shape when heated.

The I-beam-shaped fastener in figure 19(a) showed the weakest average disengagement strength. This was most likely due to plastic deformation during folding before insertion. Despite stress distribution, this fastener type lost 28% of its initial strength after four cycles. The disengagement strength can easily be enhanced by increasing the flange thickness or fine-tuning the size of the notches. These results indicate that the I-beam design rivets are favorable for places where low-profile assembly is needed with relatively weak disengagement strength.

The anchor-shaped fastener in figure 19(b) showed relatively high disengagement strength, good reusability, and easy insertion. This type lost only 16% of its initial strength after four cycles. Its design distributes stress effectively, and plastic deformation barely occurs during manual folding. This means that the rivet can be removed simply by pulling two

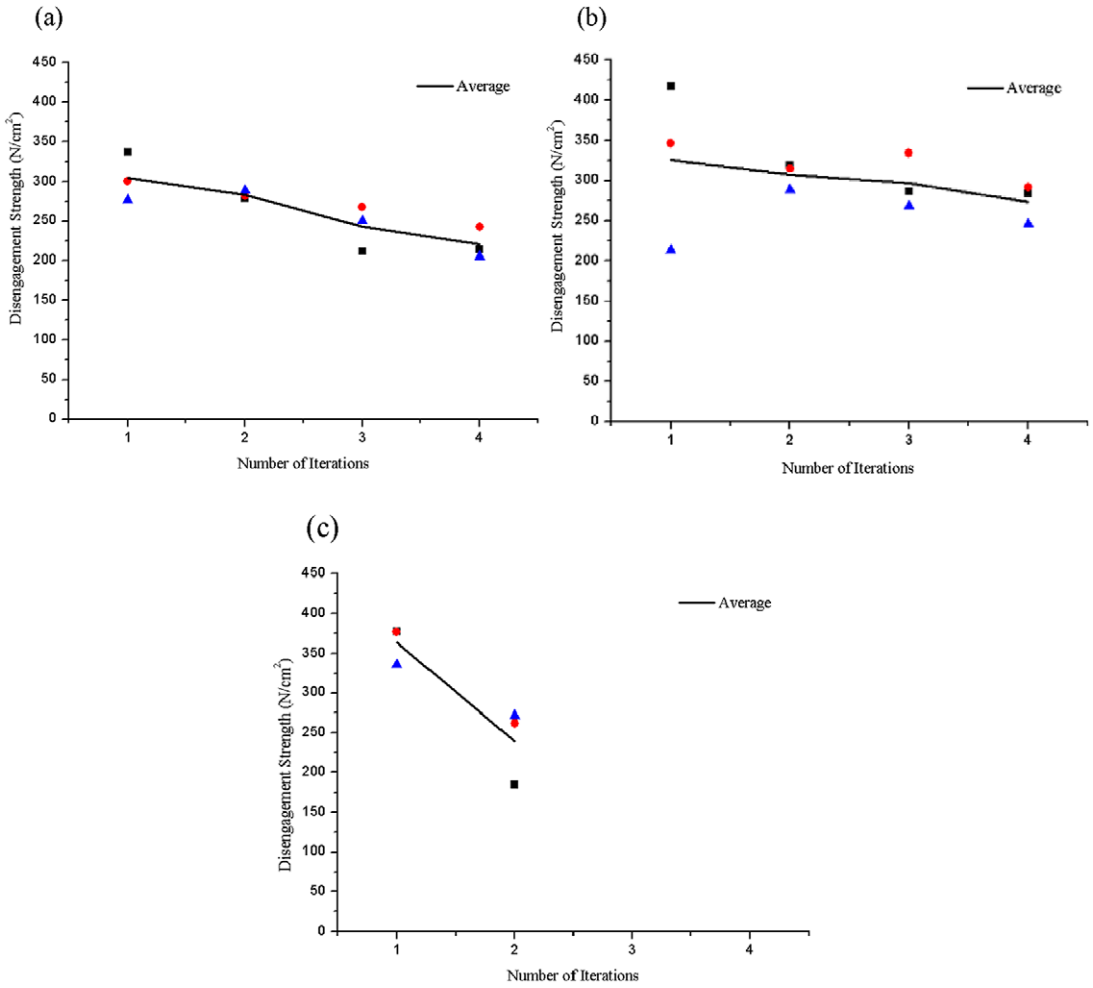

Figure 19. Measurement results of disengagement strength and reusability for (a) the I-beam-shape rivet, (b) the anchor-shape rivet, and (c) the arrow-shape rivet.

CFRP parts apart by hand and that it can be used with guaranteed strength. Its particular design, however, means that low-profile engagement would be difficult.

The arrow-shaped fastener in figure 19(c) showed the highest average initial disengagement strength, because of its special design. The flanges of this type underwent plastic deformation after disengagement and lost 34% of their initial strength. Failure occurred after two cycles with the flanges. This type may be useful for strong and semipermanent assembly.

In some cases, a single SMP rivet fastener alone may not meet the required engagement condition, or the two joined parts could rotate along the web when the hole is larger than the thickness of the web. To diversify and improve the proposed designs, some other types of rivets were made via laser machining. As shown in figures 20(a)–(d), many rivets can be monolithically connected in series, in parallel, in both series and parallel, and so on, depending on the application. Through these multiple rivets, users can control the disengagement strength and prevent undesired rotation of parts. The fold lines of these pop-up rivets are laser-cut only halfway through, and the rivets can be erected along the fold lines manually.

6. Discussion

6.1. Application

The anchor-shaped SMP fasteners were chosen for actual application because of their medium engagement strength and good reusability. As shown in figure 21, ten rivets were used to connect two legs with the body of the flea robot [24]. The 1.1 g, 2 cm-long flea robot's jumping motion is triggered by a shape memory alloy coil spring actuator, and its body can be made from a laser-machined single sheet of GFRP. Its leg stiffness, which may be a decisive factor in its jumping capability, can be adjusted by the number of stacked GFRPs. The legs of the initial version of the flea robot were attached to the body using irreversible cyanoacrylate, and the need arose for a new assembly method that using a releasable, reusable, robust connector. This need has become the major catalyst in the development of SMP rivet fasteners. SMP rivet fasteners not only facilitate the interchange process but could also enhance the reliability of the experiment because we were able to use the same body with the same actuators and weight distribution.

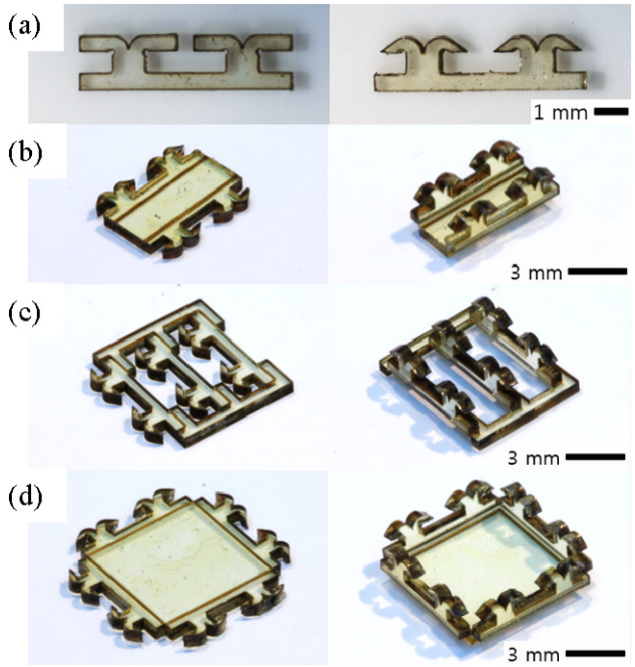

Figure 20. Various types of SMP rivets. (a) Two rivets connected in series, (b) Two double rivets connected in parallel. (c) Three double rivets connected in parallel. (d) Four double rivets connected in parallel and perpendicular arrangements.

Finally, because the SMP-based rivets recover their original shapes when heated, they can be used as blind rivets for joining two or more parts that would otherwise be impossible to join. Moreover, the weight of ten rivets is only 0.03 g, which is even lighter than cyanoacrylate (0.05 g). The rivets highlighted in the circles shown in figure 21(a) are blind rivet points. After the jumping experiments were conducted, it became clear that these rivets do not hinder the movement and endure approximately 1–2 N of disengagement force acting between the legs and the body during jumping.

6.2. Limitations

Although it shows good performance as a fastener, the SMP rivet has some limitations. It has low thermal resistance. If a microrobot using SMP rivet fasteners works in a hot environment in which the temperature rises above the glass transition temperature of the polymer, the rivet will malfunction suddenly because of the reduced Young's modulus. Moreover, users must fold the flanges beforehand, which could require cumbersome procedures if the flange width becomes too small or if too many rivets are required.

In this study, thermoplastic polyurethane SMP was used due to its good moldability, manufacturability and high shape deformation range [25]. However, thermoplastic SMPs generally have poor repeatability, are subjected to viscoelastic and viscoplastic deformations [26], and can be sensitive to moisture [23]. If the rivets can be made by other manufacturing methods [16] and machining techniques [27, 28], thermoset SMPs with better strain recovery ratios, faster strain recovery and larger shape recovery stress [29] are recommended.

Another limitation is that the single SMP rivet connects only a certain point of two parts. Comparatively, other assembly methods such as cyanoacrylate, magnets, or microconnectors [15] connect a certain area of two parts. These fasteners are able to distribute the external force over the connected area, whereas in the case of the SMP rivet fastener, the external force is concentrated on the connected point. However, this limitation may be overcome when the SMP rivets are monolithically connected in series or in parallel, as described in section 5.

7. Conclusion

We have developed a novel I-beam-shaped fastener using an SMP. The SMP fastener allows remotely triggered blind riveting, which is particularly useful in assembling microscale components. When subjected to heat, SMP fasteners become sufficiently compliant to be detached by gently moving the parts away from each other. The maximum disengagement strength and the reusability depend on the radius of the notch under the flange of the I-beam. The I-beam-shaped fasteners are designed to prevent stress concentration. The SMP rivet fastener with the smallest notch radius among samples (0.05 mm) was found to have the highest disengagement strength (150 N cm^{-2}), whereas the one with the largest

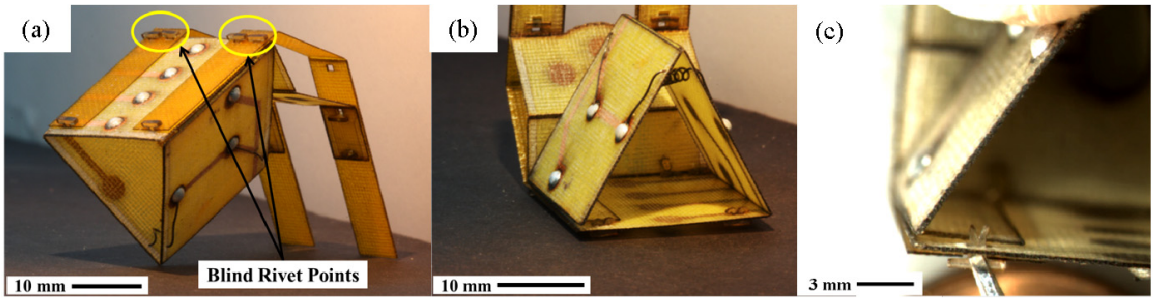

Figure 21. (a) Rivets used in connecting the legs and the body of the flea robot. The four rivets highlighted in the yellow circles indicate blind rivet points. (b) Curved flanges can be seen when the robot is upside down. (c) Magnified view of the assembly process of the leg part and the body part.

notch radius among samples (0.33 mm) showed the highest reusability, maintaining 77% of its initial disengagement strength after being reused four times. Clearly, the notch radius should be chosen to meet the disengagement strength and reusability requirements. SMP rivets have a small size, and they can be easily manufactured to various shapes; these features make them especially suitable to function as fasteners. The use of SMP rivet fasteners in microrobots allows the microrobot components to be replaced, enabling researchers to determine the optimal design and parameters, such as stiffness for the components. Furthermore, when a microrobot component malfunctions, instead of discarding the microrobot itself, it can be repaired simply by replacing the broken part. This replaceable design, which allows systematic assembly and disassembly, could change the way microrobots are built and used.

Acknowledgments

This work was supported by the National Research Foundation of Korea (NRF) grant funded by the Ministry of Education, Science and Technology (MEST) (No. 2012-0000348), and the Priority Research Centers Program (2012-041247) through the NRF funded by the MEST, Republic of Korea.

References

[1] Lendlein A and Kelch S 2002 Shape-memory polymers *Angew. Chem. Int. Edn* **41** 2034–57
[2] Cable K, Hermiller J, Kirby B and Sunday M 2009 Development of a shape memory polymer fastening system *Proc. SPIE* **7290** 72900J
[3] Stanford T, Barvosa-Carter W, Browne A L and Johnson N L 2008 Active material reversible attachments: shape memory polymer based *Proc. SPIE* **6930** 693003
[4] 2010 Shape memory fastener 20100154181 A1 pub date: Jun. 24
[5] Wood R J, Avadhanula S, Sahai R, Steltz E and Fearing R S 2008 Microrobot design using fiber reinforced composites *J. Mech. Des.* **130** 052304
[6] Sahai R, Galloway K C and Wood R J, Elastic element integration for improved flapping-wing micro air vehicle performance *IEEE Trans. Robot.* **29** 32–41
[7] Kovač M, Fuchs M, Guignard A, Zufferey J-C and Floreano D 2008 A miniature 7g jumping robot *Proc. IEEE Int. Conf. Robot. Autom.* pp 373–8
[8] Gilpin K, Kotay K, Rus D and Vasilescu I, Miche: modular shape formation by self-disassembly *Int. J. Robot. Res.* **27** 345–72
[9] Hawkes E, An B, Benbernou N M, Tanaka H, Kim S, Demaine E D, Rus D and Wood R J 2010 Programmable matter by folding **107** 12441–5
[10] Gillies A G and Fearing R S 2010 A micromolded connector for reconfigurable millirobots *J. Micromech. Microeng.* **20** 105011
[11] Messler R W Jr 2004 *Joining of Materials and Structures* (Oxford: Elsevier)
[12] Noh M, Kim S-W, An S, Koh J-S and Cho K-J, Flea-inspired catapult mechanism for miniature jumping robots *IEEE Trans. Robot.* **28** 1007–18
[13] Yu T X and Zhang L 1996 *Plastic Bending: Theory and Applications* (Singapore: World Scientific)
[14] Kachanov L M 1971 *Foundations of the Theory of Plasticity* (New York: Elsevier)
[15] Shape memory polymer [Diary]-guide for injection molding *Technical Note* Diaplex SMP Technologies Inc., www2.smptechcom/en/tech/
[16] Heckele M and Schomburg W K 2004 Review on micro molding of thermoplastic polymers *J. Micromech. Microeng.* **14** R1–14
[17] Azra C, Plummer C J G and Månson J-A E 2011 Isothermal recovery rates in shape memory polyurethanes *Smart Mater. Struct.* **20** 082002
[18] Illyefalvi-Vitéz Z 2001 Laser processing for microelectronics packaging applications *Microelectron. Reliab.* **41** 563–70
[19] Yung K C, Mei S M and Yue T M 2002 A study of the heat-affected zone in the UV YAG laser drilling of GFRP materials *J. Mater. Process. Technol.* **122** 278–85
[20] Tobushi H, Hara H, Yamada E and Hayashi S 1996 Thermomechanical properties in a thin film of shape memory polymer of polyurethane series *Smart Mater. Struct.* **5** 483–91
[21] Azra C, Plummer C J G and Månson J A E 2011 Isothermal recovery rates in shape memory polyurethanes *Smart Mater. Struct.* **20** 082002
[22] Turnbull A, Maxwell A S and Pillai S 1999 Residual stress in polymers—evaluation of measurement techniques *J. Mater. Sci.* **34** 451–9
[23] Yang B, Huang W M, Li C and Li L 2006 Effects of moisture on the thermomechanical properties of a polyurethane shape memory polymer *Polymer* **47** 1348–56
[24] Kim J-S, Jung G-P, Koh J-S and Cho K-J 2013 Meso-scale robot assembly using shape memory polymer rivet fastener *Int. Conf. Intelligent Robots and Systems (Tokyo, Nov. 3–7)* pp 2082
[25] Ward S, Pooja S, Wilson S W and Duncan M 2010 Biomedical applications of thermally activated shape memory polymers *J. Mater. Chem.* **20** 3356–66
[26] Yiping L, Ken G, Martin L D, Alan R G and Julie D 2006 Thermomechanics of shape memory polymers: uniaxial experiments and constitutive modeling *Int. J. Plast.* **22** 279–313
[27] Kim S L and Kim G M 2011 Micropatterning on roll surface using photo-lithography processes *Int. J. Precis. Eng. Manuf.* **12** 763–8
[28] Yong D Y, Da W G, Zhen J H, Xue S Z and Jiu C Y 2012 Polymer nanostructured components machined directly by the atomic force microscopy scratching method *Int. J. Precis. Eng. Manuf.* **13** 269–73
[29] Xu J and Song J 2011 *Biomedical Engineering—Frontiers and Challenges* ed R Fazel-Rezai (Croatia: InTech) chapter 6 (Thermal Responsive Shape Memory Polymers for Biomedical Applications)